Combustion Models for Wooden Brands

J. P. WOYCHEESE and P. J. PAGNI

ABSTRACT

Eight combustion models for burning brands are reviewed. An averaged stagnation-point burning model, using the chemical properties of wood, is used here. Maximum propagation distances are calculated for disk-shaped brands lofted in large fires, such as occur after earthquakes or at urban/wildland interfaces. Lofting in the fire plume and propagation downwind are approximated here with distinct flow fields: a Baum and McCaffrey model for the plume and a constant horizontal velocity driving downwind propagation. In the plume, the brands rise with maximum drag and no lift. During propagation, both lift and drag act on the brand. It is assumed to have a fixed angle of attack, $35^\circ \le \alpha \le 90^\circ$, with respect to the relative velocity vector. For these α, the disk lift and drag coefficients are $C_l = 1.17\cos(\alpha)$ and $C_d = 1.17\sin(\alpha)$, so that lift increases with decreasing α. Analytic expressions for dimensionless propagation distance, height, and brand size are developed in terms of four dimensionless parameters: initial lofting height, h_o^*; constant horizontal wind, U_w^*; angle of attack, α; and dimensionless burning parameter, Ψ.

Keywords: Post-earthquake fires, urban/wildland intermix fires, brand propagation, spotting fires.

INTRODUCTION

Burning brands, lofted above large fires and propagated by the prevailing winds, can cause spot ignitions far from the flame front. These distant and unexpected fires are an important mechanism for fire spread in post-earthquake and urban/wildland intermix fires. The 20 October Oakland Hills Fire quickly overwhelmed fire fighting efforts, in part due to brand propagation and spotting hundreds of meters ahead of the fire front [1]. Although spotting has received considerable attention from the forest fire community [2-7], little research quantifies brand propagation from structures or rubble piles.

This paper explores the brand combustion data available in the literature and applies one combustion model to determine maximum propagation distances for disk-shaped brands lofted from large, single-plume fires. The inclusion of lift forces provides greater brand travel during propagation than can be achieved by spherical or cylindrical brands. Analytic equations for brand thickness and propagation height with time are determined as functions of heat release rate, wind speed, and brand and air properties. Previous studies by Tarifa, et. al., [8, 9] and Lee,

John P. Woycheese, Patrick J. Pagni, Department of Mechanical Engineering, University of California, Berkeley, CA 94720-1740.

International Conference on Fire Research and Engineering (ICFRE3), Third (3rd). Proceedings. Society of Fire Protection Engineers (SFPE), National Institute of Standards and Technology (NIST) and International Association of Fire Safety Science (IAFSS). October 4-8, 1999, Chicago, IL, Society of Fire Protection Engineers, Boston, MA, 53-71 pp, 1999.

et al., [10, 11] assume a constant vertical velocity for lofting calculations with particles released at arbitrary heights. This paper provides a more accurate lofting height by using Baum and McCaffrey plume model [12] for axisymmetric pool fires. During propagation, the prevailing winds are approximated as constant and horizontal, and the terrain is assumed flat.

This paper is divided into four sections: Combustion Models, Dynamics, Results, and Conclusions. In the analysis, equations are developed from brand momentum balances for both the lofting and propagation phases. The dimensionless results from these equations are analyzed in the results section and summarized in the conclusions.

COMBUSTION MODELS

The heterogeneous combustion characteristics of brands, coupled with size and shape histories, are required by large eddy simulations (LES) of fire propagation to calculate fire spotting distances. Although initial brand conditions such as size, shape, and material properties can be approximated, quantifying the gravitational and aerodynamic forces during flight requires that the brand shape, size, mass, and drag and lift coefficients be known as functions of time. Prior to lofting and propagation, brands are assumed to be smooth-formed; i.e., combustion will have removed corners and other sharp edges, so that lofted brands can be approximated as spheres, disks, or cylinders. A small drag coefficient and large mass-to-cross-sectional-area ratio limits the propagation range of spheres relative to other shapes. Therefore, this paper focuses primarily on disks. There follows a brief description of combustion brand characteristics from the literature:

Albini [5, 6, 7] developed a firebrand burning-rate model that is primarily based on cylinder data from Muraszew [3]. The density and mass of brands after timed combustion periods were reported for four wood types (Ponderosa pine, western larch, western red cedar, and Engelmann spruce) and two sizes (5-cm-long, 12.5- and 25-mm-initial-diameter cylinders). The data scatter is fairly large because some of the pieces fractured during the experiments. Albini's combustion model is based on the assertion by Lee and Hellman [10] that the mass loss rate is proportional to the rate of air supplied to the surface and on his assumption that dA_c/dt, the rate of change of the cross-section, will be small compared to $d(\rho_s D)/dt$, where D is the time-dependent brand length in the direction of the wind. The resulting brand model is y=0.0064x, where $y = 1-(\rho_s D)/(\rho_s D)_o$ and $x = \rho_a U t/(\rho_s D)_o$; ρ_s is the time-dependent brand average density, U is the brand relative velocity, and the subscript "o" indicates initial conditions. Albini uses this model in several different velocity fields [5, 6, 7]. The data provided by Albini is limited to one run for each type of wood, initial size, and combustion period.

Tarifa, et al., [8, 9] have performed analytical and experimental examinations of spotting fires. In the former, the brands were assumed to be point masses, with drag acting in the direction opposite to the motion of the center of gravity; lift was not considered. The experimental phase involved two wind tunnels: one each aligned horizontally and vertically. In the horizontal wind tunnel, the brands were attached to a 2-component strain gage by a thin steel wire. No strain gage was used in the vertical wind tunnel; rather, the wind tunnel velocity was adjusted to keep the wire to which the brand was attached horizontal. Brands were ignited by a butane torch and size changes were recorded by photograph. Spheres (ϕ = 10-50 mm), cylinders (ϕ = 6-15 mm, l = 18-36 mm), and square plates (32x32x2 - 32x32x16 mm) of five different

woods (pine, oak, spruce, aspen, and balsa) were examined and the moisture content was varied from 2 – 25%. Flaming transition to glowing combustion occurred at low wind velocities and only glowing combustion was observed at high speeds.

Phillips and Becker [13] have used bark-covered pine sticks, with diameters from 9 to 50 mm, in constant, high-temperature flow between 3 and 19 m/s. The heated wind tunnel was sufficiently small that it was necessary to calculate U_∞ from the known wind-tunnel velocity, U_t. Over 150 experimental runs were performed, with five runs for each combination of velocity, temperature, and sample diameter. Temporal mass-loss curves were given for a number of cases, along with the authors' equation for mass loss. For small time,

$$\frac{m_o - m}{m_o} = 14.6 \exp\left(\frac{-3920}{T_\infty}\right) \cdot Fo \cdot Bi \tag{1}$$

where m is the instantaneous brand mass; T_∞ is the ambient temperature; Fo is the Fourier number, $\alpha_o t / B_o^2$; Bi is the Biot number, $h_o B_o / k_o$; α is the brand thermal diffusivity; k is the brand thermal conductivity; B is the brand volume-to-surface-area ratio; h is the total heat transfer coefficient; and the subscript "o" denotes initial conditions. For large time, the mass ratio was found to be

$$\frac{m_o - m}{m_o \cdot Bi} = f\left[Fo \cdot \exp\left(\frac{-3267}{T_\infty}\right)\right] \tag{2}$$

The data presented are of limited use because shape and size were not provided as functions of time. The mass-loss curves appear to have two linear regions in log-log plots that generally last until more than half of the mass has been consumed. Brands in low temperature and velocity flow stop combusting well before the brands were consumed. Becker and Phillips [14] argue that the combusting sticks consist of two zones, char and virgin wood, the radii of which decrease somewhat independently. Like Albini, Becker and Phillips believe that a constant char thickness is maintained for large-diameter sticks; for sticks with $D_o > 20$ mm, the "equilibrium" char layer was determined to be roughly 6 mm when the flow temperature was above 745 °C.

Muraszew [2] developed a model wherein both the average density and brand size decrease with time. This paradigm, coupled with Tarifa's trajectory model, correlates experimental data [8]. Muraszew notes that although C_d varies greatly at low Reynolds number, such low Re brands are likely to be too small to cause a spot fire; thus C_d is assumed to be a function of shape alone. The density was approximated by:

$$\frac{\rho(t)}{\rho_o} = \exp\left(\frac{-(t - t_{ign})}{57 \cdot D_o}\right) \quad \text{for} \quad t_{ign} \le t \le 80 \cdot D_o \tag{3}$$

where $t_{ign} = 12 \cdot D_o$, with t in seconds and D_o in cm. This equation is used with the terminal velocity data to determine the effective diameter as a function of time:

$$\frac{D(t)}{D_o} = \left(\frac{w_f(t)}{w_{f,o}}\right)^2 \cdot \left(\frac{\rho_o}{\rho(t)}\right) \tag{4}$$

where D is the time-dependent brand diameter, w_f is the brand terminal velocity, ρ is the brand density, and the subscript "o" denotes an initial value.

Tse and Fernandez-Pello [15] have developed a combustion model for spherical brands that employs a two-diameter system, for mass and size, with parameters that are empirically fit to Tarifa's mass and surface area data [8, 9]. The combustion model is used in conjunction with ambient wind to provide propagation distances for brands caused by power-line arcing near trees. The effective overall diameter, D_{eff}, determines the brand mass, assuming constant average virgin wood and char density, and decreases according to $d(D_{eff}^2)/dt = -\beta$. The wind effects on boundary layer thickness are found in $\beta = \beta_o\left(1 + 0.276\,Re^{1/2}\,Sc^{1/3}\right)$. The brand regression rate, $d(D^4)/dt = -2\sqrt{3}\beta^2 t$, couples the physical brand size, which is used to calculate drag, to the relative brand velocity through β. The brands are assumed to extinguish when the mass ratio falls to $m/m_o = 0.24$, based on a final char yield of ρ/ρ_o=0.24 from Atreya [16], after which the temperature decreases by convection and radiation from 993 K.

Woycheese and Pagni [17, 18] have developed three paradigms for brands: burning-droplet, linear regression, and stagnation-point combustion. The burning-droplet problem models a spherical fuel particle combusting in an oxidizing, quiescent atmosphere and can be adopted as a crude first approximation for spherical wooden brands. The surface regression rate is an underestimate due to the effects of forced convection. The wood is assumed to be a homogeneous solid [8] and the brand relative velocity is assumed sufficient to remove significant ash from surface combustion, although adjustment of B or ρ_s may account for a small ash layer. The regression rate of the spherical brand is

$$\frac{dD}{dt} = -4\alpha\left(\frac{\rho_a}{\rho_s}\right)\left(\frac{\ln(1+B)}{D}\right) \tag{5}$$

where α is the thermal diffusivity of air and B is the mass transfer number for wood, here assumed to be 1.2 [18]. For brands lofted in a Baum and McCaffrey plume velocity field [12], there is an initial brand size, D_{col}, that provides the maximum propagation distance, and yet is smaller than the maximum loftable size, $D_{o,max}$; thus, all brands with an initial size $D_{col} \le D_o \le D_{o,max}$ have the same maximum propagation distance.

Constant linear regression is the simplest possible combustion model; it appears to be a good approximation to some of the literature data. The change in diameter with respect to time is dD/dt=-E, where the regression rate, E, is a positive number chosen to represent the material composing the brand; Drysdale [19] suggests $E=6.6 \times 10^{-5}$ m/s for wood. This model may provide a useful approximation to the size change of many brand shapes.

The stagnation-point burning problem is useful for burning disks where the angle between the disk face and the relative wind (angle of attack, α) is near 90°. The mass flux [20] is

$$\dot{m}'' \equiv -\rho_s\left(\frac{dh}{dt}\right) = -\frac{2\rho_a|\mathbf{W}|f(0)}{\sqrt{\sigma|\mathbf{W}|/\nu}}, \tag{6}$$

where σ is the radial coordinate on the disk surface, $f(0) = -0.353r^{-0.02}B^{0.611-0.0651\ln(B)}$, r is the mass consumption number, B is the mass transfer number, and $|\mathbf{W}|$ is the magnitude of the brand velocity relative to its surroundings. Note that h refers to the brand thickness. Reference [21] defines $r = Y_{o\infty}s/Y_{fw}$ and $B = (QY_{o\infty}/\nu_o M_o - h_w)/L$, where $s = \nu_f M_f/\nu_o M_o$ and $Y_{fw} = (B - sY_{o\infty})/(1+B)$. For these equations, $Y_{o\infty}$ is the mass fraction of oxygen far from the disk, $\nu_{f,o}$ are the stoichiometric coefficients for fuel and oxygen, $M_{f,o}$ are the molecular weights of fuel and oxygen, h_w is the specific enthalpy at the disk surface, and Q is the energy released by combustion of ν_f moles of gas phase fuel. B and r are assumed to be 1.2 and 0.50 for wood [20]. To remove the infinite regression rate at the center of the disk, Eq. (6) is integrated over the surface of the brand, assuming a constant radius, R, and constant, homogeneous density, to give an average regression rate,

$$\frac{d\bar{h}}{dt} = \frac{8}{3}\left(\frac{\rho_a}{\rho_s}\right)\sqrt{\frac{|\mathbf{W}|\nu}{R}}f(0) = \frac{8}{3}\left(\frac{\rho_a}{\rho_s}\right)\sqrt{\frac{2|\mathbf{W}|\nu\varepsilon}{h_o}}f(0), \tag{7}$$

where $\varepsilon = h_o/2R$ is the length-to-diameter ratio. The inclusion of relative velocity effects into the combustion rate significantly affects the brand lifetime and maximum propagation distance; the latter is also influenced by the angle of attack

DYNAMICS

Conservation of brand momentum [22] is given by

$$\frac{d}{dt}(m\mathbf{V}) = \sum \mathbf{F}, \tag{8}$$

where m is the disk mass, **V** is its velocity with respect to ground, and **F** are the forces on the brand. If the prevailing winds are assumed to be steady and irrotational, prudent selection of axes reduces the problem to one of two dimensions, x and z, such that $\mathbf{V} = V_x\hat{\mathbf{i}} + V_z\hat{\mathbf{k}}$, where $\hat{\mathbf{i}}$ and $\hat{\mathbf{k}}$ are the unit vectors in the x and z directions, respectively. As indicated in Figure 1 Fig. 1, a disk brand in a velocity field is subjected to three forces: gravity, drag, and lift. The gravity force is

$$\mathbf{F}_g = -mg\hat{\mathbf{k}}, \tag{9}$$

with g the acceleration due to gravity, and the drag force is

$$\mathbf{F}_d = F_{d,x}\hat{\mathbf{i}} + F_{d,z}\hat{\mathbf{k}}, \tag{10}$$

where the components of the drag force are

$$F_{d,x} = \frac{1}{2} A_c \rho_a C_d |\mathbf{W}|^2 \cos(\Gamma) = \frac{1}{2} A_c \rho_a C_d |\mathbf{W}| W_x \quad \text{(a)}$$
$$F_{d,z} = \frac{1}{2} A_c \rho_a C_d |\mathbf{W}|^2 \sin(\Gamma) = \frac{1}{2} A_c \rho_a C_d |\mathbf{W}| W_z \quad \text{(b)}. \tag{11}$$

For these equations, A_c is the cross-sectional area of the brand, ρ_a is the density of air, C_d is the drag coefficient, $\mathbf{W} \equiv W_x \hat{\mathbf{i}} + W_z \hat{\mathbf{k}} = \mathbf{U} - \mathbf{V}$ is the velocity of the flow relative to the particle, and Γ is the angle between the relative velocity and the x-axis. The drag force acts in the direction of $\mathbf{W}$ with a strength proportional to the square of $|\mathbf{W}|$.

Similarly, the lift force is

$$\mathbf{F}_l = F_{l,x} \hat{\mathbf{i}} + F_{l,z} \hat{\mathbf{k}}, \tag{12}$$

where the components of the lift force are

$$F_{l,x} = \frac{1}{2} A_c \rho_a C_l |\mathbf{W}|^2 \cos(\Gamma + 90^\circ) = -\frac{1}{2} A_c \rho_a C_l |\mathbf{W}| W_z \quad \text{(a)}$$
$$F_{l,z} = \frac{1}{2} A_c \rho_a C_l |\mathbf{W}|^2 \sin(\Gamma + 90^\circ) = \frac{1}{2} A_c \rho_a C_l |\mathbf{W}| W_x \quad \text{(b)}. \tag{13}$$

Here, C_l is the lift coefficient and 90° orients the lift force perpendicular to drag. Hoerner [23] has determined lift and drag coefficients for circular disks to be

$$C_d = C_n \sin(\alpha) \quad \text{(a)}$$
$$C_l = C_n \cos(\alpha) \quad \text{(b)}, \tag{14}$$

where α is the angle of attack as shown in Fig. 1, held constant during the brand's flight, with $C_n = 1.17$ for $35^\circ \le \alpha \le 90^\circ$. Combining Eqs. (8) to (14), the momentum equations become

$$\frac{d}{dt}(mV_x) = \frac{1}{2} A_c \rho_a |\mathbf{W}| C_n (\sin(\alpha) W_x - \cos(\alpha) W_z) \quad \text{(a)}$$
$$\frac{d}{dt}(mV_z) = \frac{1}{2} A_c \rho_a |\mathbf{W}| C_n (\sin(\alpha) W_z + \cos(\alpha) W_x) - mg \quad \text{(b)}. \tag{15}$$

Using $m = \pi d^2 h \rho_s / 4$ and $A_c = \pi d^2 / 4$, where d is the disk diameter, h is its height, and ρ_s is its average density, Eqs. (15) can be solved for the acceleration equations,

$$\frac{dV_x}{dt} = \frac{1}{2}\left(\frac{\rho_a}{\rho_s}\right)\left(\frac{C_n |\mathbf{W}|}{h}\right)(\sin(\alpha) W_x - \cos(\alpha) W_z) - \frac{V_x}{h}\left(\frac{d\bar{h}}{dt}\right) \quad \text{(a)}$$
$$\frac{dV_z}{dt} = \frac{1}{2}\left(\frac{\rho_a}{\rho_s}\right)\left(\frac{C_n |\mathbf{W}|}{h}\right)(\sin(\alpha) W_z + \cos(\alpha) W_x) - \frac{V_z}{h}\left(\frac{d\bar{h}}{dt}\right) - g \quad \text{(b)}. \tag{16}$$

The terms on the right-hand side correspond to acceleration due to drag, lift, and mass loss ($dm/dt \le 0 \ \forall\, t$). The additional vertical term gives deceleration due to gravity.

The propagation problem consists of three phases: lofting, downwind propagation, and deposition or burnout. The first two phases are approximated as completely separate for this paper. During lofting, the brand follows the centerline of the plume, which is assumed to be vertical. For maximum loft, α is assumed to be constant at 90°. The plume velocity, U_{bm}, is based on the Baum and McCaffrey plume model [12], so that the relative velocity of the brand within the plume is

$$\mathbf{W}_{plume} = (-V_x)\hat{\mathbf{i}} + (U_{bm} - V_z)\hat{\mathbf{k}}. \tag{17}$$

For propagation, the brand is removed from the plume at the height that results in maximum spotting distance – removal at greater heights results in burn-out above the ground and at lower heights in smaller propagation distances – and is immersed in the velocity field of the ambient wind. The wind above and around a large fire is a complex function of terrain, atmospheric conditions, and fire size. This study is intended to provide limiting cases for the maximum propagation of burning brands; therefore, following Tarifa, et al.,[8] a high-velocity, constant, horizontal wind is used. The relative velocity during propagation is

$$\mathbf{W}_{prop} = (U_w - V_x)\hat{\mathbf{i}} - V_z\hat{\mathbf{k}}, \tag{18}$$

where U_w is the constant velocity of the ambient wind.

The lofting and propagation problem has five dependent variables, V_x, V_z, x, z, and h, and one independent variable, t; the brand characteristics, angle of attack, and horizontal wind are parameters. The brand is assumed to begin lofting at t=0 with V_x, V_z, and x initially zero and the initial brand thickness, h_o, known. The initial brand height is the only condition not known *a priori*. For each initial brand size in the Baum and McCaffrey plume model, however, there is a unique initial height, z_o, below which gravity exceeds drag. (During the lofting phase, it is assumed that $\alpha = 90°$, so that there is no lift force.) Brands are lofted when drag exceeds gravity, so that the minimum lofting height will occur where these two forces balance. With brand and wind velocities initially zero, $\mathbf{W} = U_{bm}\hat{\mathbf{k}} = 2.13U_c(z/z_c)^{1/2}$ in the flame, where U_c and z_c are the characteristic velocity and height of the Baum and McCaffrey plume,

$$\begin{aligned} U_c &= \left(\left(\dot{Q}_o g^2\right)/\left(\rho_a c_p T_\infty\right)\right)^{1/5} \quad \text{(a)} \\ z_c &= \left(\dot{Q}_o/\left(\rho_a c_p T_\infty \sqrt{g}\right)\right)^{2/5} \quad \text{(b).} \end{aligned} \tag{19}$$

Here, $\dot{Q}_o$ is the fire heat release rate, c_p is the specific heat of air, and T_∞ is the ambient air temperature. Assuming that $\alpha = 90°$ for maximum loft, Eqs. (16) reduce to

$$\begin{aligned} \frac{dV_x}{dt} &= 0 \quad \text{(a)} \\ \frac{dV_z}{dt} &= \frac{1}{2}\left(\frac{\rho_a}{\rho_s}\right)\left(\frac{C_n}{h_o}\right)\left(2.13U_c\left(\frac{z_o}{z_c}\right)^{1/2}\right)^2 - g \quad \text{(b).} \end{aligned} \tag{20}$$

Solving Eqs. (20) for z_o, assuming that $dV_z/dt = 0$ at t=0, gives

$$z_o = \left(\frac{2gh_o z_c}{C_n (2.13U_c)^2} \right) \left(\frac{\rho_s}{\rho_a} \right) \tag{21}$$

The brands are assumed to launch from this minimum height. Similarly, the maximum loftable disk thickness can be found by solving Eqs. (20) with the maximum plume velocity, $U_{bm} = 2.45U_c$, which occurs at $z_o = 1.32$. With $dV_z/dt = 0$ at t=0,

$$h_{o,max} = \frac{1}{2} \left(\frac{\rho_a}{\rho_s} \right) \frac{C_n (2.45U_c)^2}{g}. \tag{22}$$

The equations to be solved are

$$\frac{dV_x}{dt} = \frac{1}{2} \left(\frac{\rho_a}{\rho_s} \right) \left(\frac{C_n \sqrt{(U_x - V_x)^2 + (U_z - V_z)^2}}{h} \right) \left(\sin(\alpha)(U_x - V_x) - \cos(\alpha)(U_z - V_z) \right) - \frac{V_x}{h} \left(\frac{dh}{dt} \right) \tag{a}$$

$$\frac{dV_z}{dt} = \frac{1}{2} \left(\frac{\rho_a}{\rho_s} \right) \left(\frac{C_n \sqrt{(U_x - V_x)^2 + (U_z - V_z)^2}}{h} \right) \left(\sin(\alpha)(U_z - V_z) + \cos(\alpha)(U_x - V_x) \right) - \frac{V_z}{h} \left(\frac{dh}{dt} \right) - g \tag{b}$$

$$\frac{dx}{dt} = V_x \tag{c}$$

$$\frac{dz}{dt} = V_z \tag{d}$$

$$\frac{dh}{dt} = -\frac{8}{3} \left(\frac{\rho_a}{\rho_s} \right) \sqrt{\frac{2\sqrt{(U_x - V_x)^2 + (U_z - V_z)^2} \nu \varepsilon}{h_o}} \left(-f(0) \right) \tag{e},$$

where, during lofting, $U_x = 0$ and $U_z = U_{bm}$, and during propagation, $U_x = U_w$ and $U_z = 0$. Except for a brief startup period during lofting, the change in mass and thickness is slow enough to allow the brand velocity to adjust to keep the external forces on the brand nearly in balance at all times. This allows approximate expressions for the relative velocity to be obtained by assuming, following Tarifa, et al.,[8] that the external forces are balanced. With $dV_{x,z}/dt + (V_{x,z}/h)(dh/dt) = 0$, which is synonymous to $\sum \mathbf{F} = 0$, Eqs. (23)a and b reduce to

$$W_z = W_x \tan(\alpha) \tag{a}$$

$$W_z \sin(\alpha) + W_x \cos(\alpha) = 2g \left(\frac{\rho_a}{\rho_s} \right) \left(\frac{h}{C_n |\mathbf{W}|} \right) \tag{b}$$

Rearranging Eq. (24)b and using Eq. (24)a yields

$$W_x = \left(\frac{2}{\sin^2(\alpha) + \cos^2(\alpha)} \right) \left(\frac{\rho_s}{\rho_a} \right) \left(\frac{hg \cos(\alpha)}{|\mathbf{W}|} \right) \tag{25}$$

The relative velocities in the x- and z-directions are determined from Eqs. (24)a and (25),

$$W_x = 2\left(\frac{\rho_s}{\rho_a}\right)\left(\frac{hg\cos(\alpha)}{|W|}\right) \qquad \text{(a)}$$
$$W_z = 2\left(\frac{\rho_s}{\rho_a}\right)\left(\frac{hg\sin(\alpha)}{|W|}\right) \qquad \text{(b)}. \qquad \textbf{(26)}$$

Using $|W| = \sqrt{(W_x)^2 + (W_z)^2}$, the relative velocity is

$$|W| = \sqrt{2\left(\frac{\rho_s}{\rho_a}\right)hg}, \qquad \textbf{(27)}$$

so that $W_x = \cos(\alpha)\sqrt{2\rho_s hg/\rho_a}$ and $W_z = \sin(\alpha)\sqrt{2\rho_s hg/\rho_a}$.

Equation (27) is substituted into Eq. (23)e to give an approximate equation for the brand thickness history,

$$\frac{dh}{dt} = -\frac{8}{3}\left(\frac{\rho_a}{\rho_s}\right)\left(\frac{2\nu\varepsilon}{h_o}\right)^{1/2}\left(\frac{2\rho_s hg}{\rho_a}\right)^{1/4}(-f(0)) \qquad \textbf{(28)}$$

which is separated and integrated, using $h=h_o$ at $t=0$, to give the brand thickness,

$$h = \left(h_o^{3/4} - 2^{7/4}\left(\frac{\rho_a}{\rho_s}\right)^{3/4}\left(\frac{\nu\varepsilon}{h_o}\right)^{1/2} g^{1/4}(-f(0))t\right)^{4/3}. \qquad \textbf{(29)}$$

Solving for t with h=0 gives the burnout time,

$$t_b = \frac{h_o^{3/4}}{2^{7/4}\left(\frac{\rho_a}{\rho_s}\right)^{3/4}\left(\frac{\nu\varepsilon}{h_o}\right)^{1/2} g^{14}(-f(0))}. \qquad \textbf{(30)}$$

For the propagation phase, it is convenient to define a time, t_p, such that $t_p = 0$ when the brand is removed from the plume. Then,

$$h_p = \left(h_{p,o}^{3/4} - 2^{7/4}\left(\frac{\rho_a}{\rho_s}\right)^{3/4}\left(\frac{\nu\varepsilon}{h_o}\right)^{1/2} g^{1/4}(-f(0))t_p\right)^{4/3} \qquad \textbf{(31)}$$

where $h_p(t_p)$ is the brand size during propagation and $h_{p,o}$ is the thickness at brand removal from the plume. The time to burnout during propagation is then obtained by setting $h_p = 0$,

$$t_{p,b} = \frac{h_{p,o}^{3/4}}{2^{7/4}\left(\frac{\rho_a}{\rho_s}\right)^{3/4}\left(\frac{\nu\varepsilon}{h_o}\right)^{1/2} g^{1/4}(-f(0))} \qquad \textbf{(32)}$$

The brand height during lofting cannot be determined analytically due to the dependence of U_{bm} on height. During propagation, however, $U_z \approx 0$; thus an approximate equation for brand height can be found from Eqs. (23)d, (27), and (29),

$$\frac{dz_p}{dt_p} = -\left(\frac{2g\rho_s}{\rho_a}\right)^{1/2}\left(h_{p,o}^{3/4} - 2^{7/4}\left(\frac{\rho_a}{\rho_s}\right)^{3/4}\left(\frac{\nu\varepsilon}{h_o}\right)^{1/2} g^{1/4}\left(-f(0)\right)t_p\right)^{2/3} \sin(\alpha). \tag{33}$$

Integrating Eq. (33), with $z_p=0$ at $t_p=t_{p,b}$, brand height during propagation is

$$z_p = \frac{3}{10}\left(\frac{\left(\frac{\rho_a}{\rho_s}\right)^{5/4}\left(\frac{h_o^2 g}{2\nu^3\varepsilon^2}\right)^{1/4}}{-f(0)}\right)\left(h_{p,o}^{3/4} - 2^{7/4}\left(\frac{\rho_a}{\rho_s}\right)^{3/4}\left(\frac{\nu\varepsilon}{h_o}\right)^{1/2} g^{1/4}\left(-f(0)\right)t_p\right)^{5/3} \sin(\alpha) \tag{34}$$

A similar strategy can be used to develop an analytic expression for the propagation distance. There is no horizontal wind during lofting, but after the brand is ejected from the plume, $U_x = U_w$, which is assumed constant. Equations (23)c, (27), and (29) are used with U_w to find a differential equation for propagation

$$\frac{dx_p}{dt_p} = U_w - \left(\frac{2g\rho_s}{\rho_a}\right)^{1/2}\left(h_{p,o}^{3/4} - 2^{7/4}\left(\frac{\rho_a}{\rho_s}\right)^{3/4}\left(\frac{\nu\varepsilon}{h_o}\right)^{1/2} g^{1/4}\left(-f(0)\right)t_p\right)^{2/3} \cos(\alpha) \tag{35}$$

Integrating, with $x_p=0$ at $t_p=0$, gives

$$x_p = \left(\frac{3\left(\frac{\rho_a}{\rho_s}\right)^{5/4}\left(\frac{h_o^2 g}{2\nu^3\varepsilon^2}\right)^{1/4}}{10\left(-f(0)\right)}\right)\left(h_{p,o}^{3/4} - 2^{7/4}\left(\frac{\rho_a}{\rho_s}\right)^{3/4}\left(\frac{\nu\varepsilon}{h_o}\right)^{1/2} g^{1/4}\left(-f(0)\right)t_p\right)^{5/3} - h_{p,o}^{5/4}\cos(\alpha) + U_w t_p \tag{36}$$

Although a constant velocity is used here, any integrable velocity profile is valid for substitution in Eq. (35).

NON-DIMENSIONALIZATION

Rendering equations dimensionless enables the extraction of maximum information from the minimum number of parameters. Each equation from the analysis section is non-dimensionalized using the following variables

$$\mathbf{V}^* = \frac{\mathbf{V}}{U_c} \quad \mathbf{W}^* = \frac{\mathbf{W}}{U_c} \quad \mathbf{U}^* = \frac{\mathbf{U}}{U_c} \quad U_p^* = \frac{U_w}{U_c} \quad U_w^* = \frac{U_w}{U_c}$$
$$z^* = \frac{z}{z_c} \quad x^* = \frac{x}{z_c} \quad h^* = \frac{h}{h_c} \quad t^* = \frac{t}{t_c} \tag{37}$$

where U_c and z_c are defined by Eq. (19) and $t_c = z_c/U_c$ from Eq. (23)d; the characteristic thickness will be determined in the non-dimensionalization process.

Substituting Eqs. (37) into Eqs. (23)a and b yields

$$\frac{dV_x^*}{dt^*} = \frac{1}{2}\left(\frac{\rho_a}{\rho_s}\right)\left(\frac{C_n|W^*|}{h^*}\right)\left(\frac{t_c U_c}{h_c}\right)\left(\sin(\alpha)W_x^* - \cos(\alpha)W_z^*\right) - \frac{V_x^*}{h^*}\left(\frac{dh^*}{dt^*}\right) \quad \text{(a)}$$
$$\frac{dV_z^*}{dt^*} = \frac{1}{2}\left(\frac{\rho_a}{\rho_s}\right)\left(\frac{C_n|W^*|}{h^*}\right)\left(\frac{t_c U_c}{h_c}\right)\left(\sin(\alpha)W_z^* + \cos(\alpha)W_x^*\right) - \frac{V_z^*}{h^*}\left(\frac{dh^*}{dt^*}\right) - 1 \quad \text{(b).} \tag{38}$$

From these equations, the characteristic length is

$$h_c = \left(\frac{1}{2}\right)\left(\frac{\rho_a}{\rho_s}\right)\left(C_n t_c U_c\right) = \left(\frac{C_n}{2}\right)\left(\frac{\rho_a}{\rho_s}\right)\left(\frac{\dot{Q}_o}{\rho_a c_p T_\infty \sqrt{g}}\right)^{2/5} \tag{39}$$

This is similar to the characteristic diameter found for spheres [17]. The dimensionless brand acceleration equations are therefore

$$\frac{dV_x^*}{dt^*} = \left(\frac{|W^*|}{h^*}\right)\left(\sin(\alpha)W_x^* - \cos(\alpha)W_z^*\right) - \frac{V_x^*}{h^*}\left(\frac{dh^*}{dt^*}\right) \quad \text{(a)}$$
$$\frac{dV_z^*}{dt^*} = \left(\frac{|W^*|}{h^*}\right)\left(\sin(\alpha)W_z^* + \cos(\alpha)W_x^*\right) - \frac{V_z^*}{h^*}\left(\frac{dh^*}{dt^*}\right) - 1 \quad \text{(b)} \tag{40}$$

The corresponding dimensionless brand regression rate, from Eq. (7), is

$$\frac{dh^*}{dt^*} = -\Psi\sqrt{\frac{|W^*|}{h_o^*}}, \tag{41}$$

where

$$\Psi = -f(0)\left(\frac{32}{3}\right)\left(\frac{\nu\varepsilon\rho_s g}{\rho_a C_n^3 U_c^3}\right)^{1/2} = \left(0.353r^{-0.02}B^{0.611-0.0651\ln(B)}\right)\left(\frac{32}{3}\right)\left(\frac{\nu\varepsilon\rho_s g}{\rho_a C_n^3}\right)^{1/2}\left(\frac{\rho_a c_p T_\infty}{\dot{Q}_o g^2}\right)^{3/10} \tag{42}$$

is a burning parameter based on the stagnation-point burning problem [20]; regression rates for $\Psi = 0.01$ and 0.005, for $h_o^* = 2$ and 6, are shown in Fig. 2.

The equations for height and distance become

$$\frac{dx^*}{dt^*} = V_x^* \quad \text{(a)}$$
$$\frac{dz^*}{dt^*} = V_z^* \quad \text{(b)} \tag{43}$$

Equations (40), (41), and (43) are solved simultaneously in each of the two regimes, lofting and propagation.

During lofting, $\mathbf{W}^* = -V_x^*\hat{\mathbf{i}} + (U_{bm}^* - V_z^*)\hat{\mathbf{k}}$, while during propagation, $\mathbf{W}^* = (U_w^* - V_x^*)\hat{\mathbf{i}} - V_z^*\hat{\mathbf{k}}$. The dimensionless initial conditions for lofting are $x^*(t^* = 0) = 0$, $z^*(0) = z_0^* = 0.22(h_o^*)$, $V_x^*(0) = V_z^*(0) = 0$, and $h^*(0) = h_0^*$, where the minimum initial lofting height was determined by non-dimensionalizing Eq. (21). The initial conditions for propagation will be developed following the non-dimensionalization of the analytic equations, below. The maximum loftable brand thickness, from Eq. (22), is $h_{o,max}^* = 6$, which is equal to the maximum dimensionless loftable diameter for a spherical brand.

Using Eq. (37) and the definitions for the characteristic quantities, the approximate analytic equations are also made dimensionless. The equations for relative velocity become

$$\begin{aligned} |\mathbf{W}^*| &= \sqrt{h^*} && \text{(a)} \\ W_x^* &= \sqrt{h^*}\cos(\alpha) && \text{(b)} \\ W_z^* &= \sqrt{h^*}\sin(\alpha) && \text{(c).} \end{aligned} \tag{44}$$

The dimensionless brand thicknesses during lofting and propagation are

$$\begin{aligned} h^* &= \left((h_o^*)^{3/4} + \frac{3\Psi t^*}{4\sqrt{h_o^*}} \right)^{4/3} && \text{(a)} \\ h_p^* &= \left((h_{p,o}^*)^{3/4} + \frac{3\Psi t_p^*}{4\sqrt{h_o^*}} \right)^{4/3} && \text{(b),} \end{aligned} \tag{45}$$

and the equations for propagation height and distance are

$$\begin{aligned} z_p^* &= -\frac{4}{5}\left(\frac{\sqrt{h_o^*}}{\Psi}\right)\left((h_{p,o}^*)^{3/4} + \frac{3\Psi t_p^*}{4\sqrt{h_o^*}} \right)^{5/3}\cos(\alpha) && \text{(a)} \\ x_p^* &= U_w^* t_p^* - \frac{4}{5}\left(\frac{\sqrt{h_o^*}}{\Psi}\right)\left[\left((h_{p,o}^*)^{3/4} + \frac{3\Psi t_p^*}{4\sqrt{h_o^*}} \right)^{5/3} - (h_{p,o}^*)^{5/4} \right]\sin(\alpha) && \text{(b).} \end{aligned} \tag{46}$$

The time to burnout, in the plume or during propagation, can be calculated from

$$\begin{aligned} t_b^* &= \frac{4(h_o^*)^{5/4}}{-3\Psi} && \text{(a)} \\ \text{or} \quad t_{p,b}^* &= \frac{4(h_{p,o}^*)^{3/4}\sqrt{h_o^*}}{-3\Psi} && \text{(b).} \end{aligned} \tag{47}$$

The initial conditions for propagation are $z^*(t_p^* = 0) = z_{p,o}^*$, $x^*(0) = 0$, $h^*(0) = h_{p,o}^*$, $V_x^*(0) = U_w^* - \sqrt{h_o^*}\cos(\alpha)$, and $V_z^*(0) = -\sqrt{h_o^*}\sin(\alpha)$, where the initial propagation velocities follow from Eqs. (44). Relative velocities during propagation, as determined numerically, are shown in Fig. 3, plotted against the analytic estimates based on $\sqrt{h_o^*}$. The relative velocity, $|W^*| = \sqrt{(W_x^*)^2 + (W_z^*)^2}$, is the solid line, while the x- and z-components are the dashed and dash-dot lines, respectively. The analytic solutions, from Eqs. (44), are the dotted lines near each of the three aforementioned curves. It is clear that, although the analytic solution tracks the magnitude of the relative velocity extremely well, the velocity in the x-direction is overestimated and that the velocity in the z-direction is underestimated to compensate. These differences most likely occur because the angle of the relative velocity vector, Γ, and the angle of attack, α, cannot be equal at all times if α is fixed. The relative velocity in the x-direction decreases faster than that in the z-direction; as a result, Γ increases with time. The external forces in the x-direction decrease, slowing the brand's progress. The final relative velocities in Fig. 3 are non-zero because the brand is assumed to have a small residual mass upon landing, as would be needed to supply the required ignition energy.

RESULTS

The propagation results for combusting, disk-shaped brands are presented in this section. Similar results for spherical brands have been reported elsewhere [17]. The regression rate for brand thickness is based on a stagnation-point combustion model for brands with constant radius and density. Brands are lofted from their minimum initial height in the plume to find the relationship between height and thickness. The launching height and propagation distance are determined by removing the brands from the plume at the maximum height from which they can return to the ground while still burning. Brands released from greater heights will be smaller, and thus will completely combust in the air; lower heights provide larger brands at impact and thus result in shorter propagation distances.

In previous work [17], the selection of the initial propagation size required iteration. The brand's launching height was adjusted until the maximum propagation distance was realized. Here, it is possible to determine the initial propagation height and size without iteration, using the analytic equations for propagation, in conjunction with the numerical results for lofting. Figure 4 provides the brand thickness as a function of height in the lofting phase. The initial propagation height, which is has a one-to-one correspondence to h_o^*, is provided by Eq. (46)a, with $t_p = 0$. The point at which the lofting and initial propagation heights intersect determines the height from which a brand can leave the plume and reach the ground with negligible mass, as shown in the inset of Fig. 4. The dimensionless initial propagation thickness, $h_{p,o}^*$, is given in Fig. 5 as a function of h_o^*, Ψ, and α. After the initial propagation height and thickness have been determined, the analytic equations can be solved for brand propagation height, thickness, and distance as functions of time. As shown in Fig. 6, the agreement between the maximum propagation distances determined numerically and analytically is quite good. The analytic

solution for $\Psi = 0.005$ is within a fraction of a percent of the numeric values. Thus, an approximate maximum propagation distance can be calculated analytically.

The dimensionless initial propagation thickness is a function of α, Ψ, and h_o^*; there is no dependence on U_w^*. These thicknesses, ratioed to the thickness for $\Psi = 0.01$, are only a functic of Ψ for $h_o^* \geq 2$, as

$$\frac{h_{p,o}^*}{h_{p,o_{\Psi=0.01}}^*} = 5.33(\Psi)^{0.364}, \tag{48}$$

which is valid for $0.003 \leq \Psi \leq 0.03$. Using Eq. (48) in conjunction with $h_{p,o}^*(h_o^*)$ for $\Psi = 0.01$ from Fig. 5 enables the calculation of the dimensionless initial propagation thickness. The dimensionless propagation thickness, height, and distance can be determined from Eqs. (45) to (47) once the initial propagation thickness is known.

The dimensionless maximum propagation distance, x_{max}^*, is a function of α, Ψ, h_o^*, and U_w^*, as shown in Figs. 7 through 9. Figure 7 illustrates the effects of α and h_o^* on x_{max}^*; greater distances are achieved with larger brand sizes and smaller angles of attack, as expected. The largest propagation occurs for $\alpha = 35^\circ$, the smallest angle for which the assumption of a constant normal coefficient is valid [23]. Figures 8 and 9 provide three-dimensional representations of x_{max}^* as functions of Ψ and h_o^* for $\alpha = 35^\circ$. The distances shown in Fig. 8, for $U_w^* = 4$, are approximately twice as far as those in Fig. 9, for $U_w^* = 2$.

CONCLUSIONS

Brand momentum conservation was used to determine the maximum propagation distances of wooden, disk-shaped brands lofted on the centerline of an axisymmetric pool fire in a constant horizontal wind. Brand thickness was assumed to decrease according to a regression rate from axisymmetric stagnation-point burning. Numerical solutions were used in the plume since the centerline velocity depends on height. During propagation, analytic expressions were developed since the ambient wind is assumed constant. Dimensionless maximum propagation distances were determined for a range of dimensionless initial thickness, $h_o^* \leq 6$; burning parameter, $0.003 \leq \Psi \leq 0.03$; ambient wind, $U_w^* \leq 4$; and angle of attack, $35^\circ \leq \alpha \leq 90^\circ$.

A dimensionless propagation distance of $x^* = 1350$ was obtained for the maximum dimensionless initial lofting thickness, $h_o^* = 6$, in a constant dimensionless ambient wind, $U_w^* = 4$, at a constant angle of attack, $\alpha = 35^\circ$, with an average dimensionless burning parameter, $\Psi = 0.01$. This corresponds to a propagation distance of approximately 7.9 km for a wooden disk with an initial thickness of 7.4 cm and an initial aspect ratio of 10:1. The brand is lofted above a 90 MW fire and propagates in a constant 30 m/s wind. The large propagation

distance is much greater than that for spherical brands [17], and illustrates the added spotting danger provided by lift associated with aerodynamic brands.

Future work will implement burning models for various brand shapes developed from wind-tunnel experiments. These brands will be inserted as Lagrangian particles into LES fire plume models [24-26], which describe the interaction of the flow field from large fires with complex terrain and ambient winds.

ACKNOWLEDGEMENTS

We are grateful for the continuing financial support provided by the Building and Fire Research Laboratory of the National Institute of Standards and Technology, U.S.D.O.C., under Grant No. 60NANB8D0094, and by a student grant from the Educational and Scientific Foundation of the Society of Fire Protection Engineers.

REFERENCES

1. Pagni, P.J., "Causes of the 20th October 1991 Oakland Hills Conflagration," *Fire Safety Journal*, **21**:4, 331-340, 1993.
2. Muraszew, A., "Firebrand Phenomena," *Aerospace Report No. ATR – 74 (8165 –01) –1*, The Aerospace Corporation, El Segundo, 1974.
3. Muraszew, A., Fedele, J.B., and Kuby, W.C., "Firebrand Investigation," *Aerospace Report ATR-75 (7470) –1*, The Aerospace Corp., El Segundo, CA, 1975.
4. Muraszew, A., and Fedele, J.B., "Statistical Model for Spot Fire Hazard," *Aerospace Report No. ATR – 77 (7588) –1*, The Aerospace Corporation, El Segundo, 1976.
5. Albini, F.A., "Spot Fire Distance From Burning Trees: A Predictive Model," *General Technical Report No. INT – 56*, USDA Forest Service Intermountain Forest and Range Experiment Station, Ogden, UT, 1979.
6. Albini, F.A., "Potential Spotting Distance from Wind-Driven Surface Fires," *USDA Forest Service Research Paper INT-309*, USDA, 1983.
7. Albini, F.A., "Transport of Firebrands by Line Thermals," *Combustion Science and Technology*, **32**, 277-288, 1983.
8. Tarifa, C.S., del Notario, P.P., and Moreno, F.G., "On the Flight Paths and Lifetimes of Burning Particles of Wood," *Tenth Symposium (International) on Combustion*, 1021-1037, The Combustion Institute, 1965.
9. Tarifa, C.S., del Notario, P.P., Moreno, F.G., and Vill, A.R., "Transport and Combustion of Firebrands," *Final Report of Grants FG-SP-114 and FG-SP-146*, Vol. 2, USDA, Madrid, 1967.
10. Lee, S.-L., and Hellman, J.M., "Firebrand Trajectory Study Using an Empirical Velocity-Dependent Burning Law," *Combustion and Flame*, **15**:3, 265-274, 1970.
11. Lee, S.-L., and Hellman, J.M., "Study of Firebrand Trajectories in a Turbulent Swirling Natural Convection Plume," *Combustion and Flame*, **13**:6, 645-655, 1989.
12. Baum, H.R. and McCaffrey, B.J., "Fire-Induced Flow – Theory and Experiment," *Fire Safety Science, Proceedings of the Second International Symposium*, ed. T. Wakamatsa et al., 129-148, Hemisphere, Washington, D.C., 1989.
13. Phillips, A.M., and Becker, H.A., "Pyrolysis and Burning of Single Sticks of Pine in a Uniform Field of Temperature, Gas Composition, and Gas Velocity," *Combustion and Flame*, **46**, pp. 221-251, The Combustion Institute, 1982.
14. Becker, H.A., and Phillips, A.M., "Burning of Pine in Wind at 357-857 C and 3-18 m/s: The Wave Propagation Period," *Combustion and Flame*, **58**, pp. 273-289, The Combustion Institute, 1984.
15. Tse, S.D., and Fernandez-Pello, A.C., "On the Flight Paths of Metal Particles and Embers Generated by Power Lines in High Winds – A Potential Source of Wildland Fires," *Fire Safety Journal*, **30**:4, pp. 333-356, 1998.
16. Atreya, A., "Pyrolysis, Ignition, and Fire Spread on Horizontal Surfaces of Wood," *Ph.D. Thesis*, Harvard University, Cambridge, 1983.

17. Woycheese, J.P., Pagni, P.J., and Liepmann, D., " Brand Propagation From Large-Scale Fires," *Journal of Fire Protection Engineering*, 1998, in review.
18. Woycheese, J.P., Pagni, P.J., and Liepmann, D., "Brand Lofting Above Large-Scale Fires," *Proceedings of the Second International Conference on Fire Research and Engineering*, 137-150, Society of Fire Protection Engineers, Washington, 1998.
19. Drysdale, D.D., *An Introduction to Fire Dynamics*, John Wiley and Sons, New York, 1985.
20. Kinoshita, C.M., Pagni, P.J., and Beier, R.A., "Opposed Flow Diffusion Flame Extensions," *Eighteenth Symposium (International) on Combustion*, pp. 1853-1860, The Combustion Institute, 1981.
21. Pagni, P.J., "Diffusion Flame Analyses," *Fire Safety Journal*, **3**, pp. 273-285, 1980/81.
22. Taylor, G.I., "Notes on Possible Equipment and Techniques for Experiments on Icing of Aircraft," *Journal of Aerospace Sciences*, **25**, 464, 1958.
23. Hoerner, S.F., *Fluid-Dynamic Drag*, Published by author, 1958.
24. McGrattan, K.B., Ferek, R.J., and Uthe, E.E., "Smoke Plume Trajectory from In Situ Burning of Crude Oil – Field Experiments," *Proceedings of the First International Conference on Fire Research and Engineering*, ed. D. Peter Lund, 47-52, Society of Fire Protection Engineers, Orlando, FL, 1995.
25. McGrattan, K.B., Rehm, R.G., Tang, H.C., and Baum, H.R., "A Boussinesq Algorithm for Buoyant Convection in Polygonal Domains," *NISTIR 4831*, National Institute of Standards and Technology, Gaithersburg, MD, 1992.
26. McGrattan, K.B., Baum, H.R., Walton, W.D., and Trelles, J., "., "Smoke Plume Trajectory from In Situ Burning of Crude Oil in Alaska – Field Experiments and Modeling of Complex Terrain," *NISTIR 5958*, National Institute of Standards and Technology, Gaithersburg, MD, 1997.

FIGURES

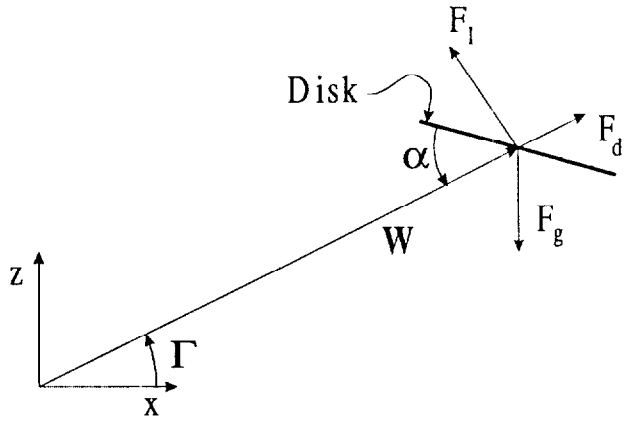

Figure 1 Schematic of the external forces on a disk brand in a velocity field.

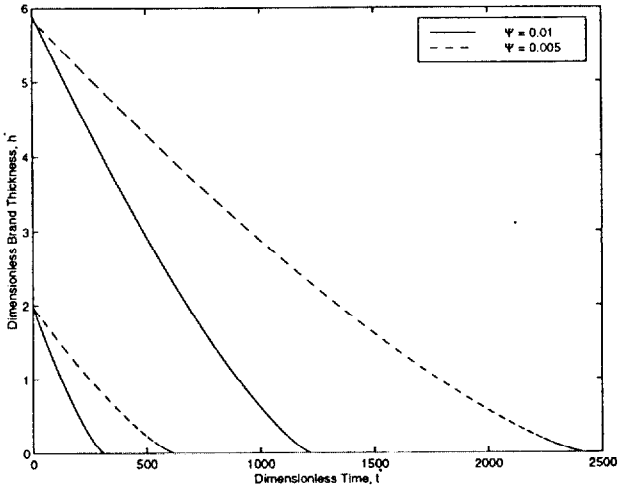

Figure 2 Dimensionless brand thickness as a function of dimensionless time for two initial thicknesses and two Ψ, as determined from the stagnation-point burning model.

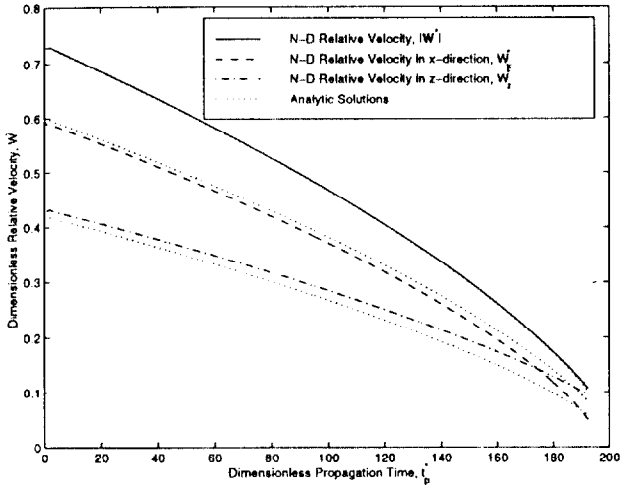

Figure 3 Comparison of numerically calculated relative velocities to the approximate analytic expressions involving $\sqrt{h_o^*}$. The relative velocities shown are for the propagation of a disk brand with $\alpha = 35°$, $h_o^* = 6$, $U_w^* = 4$, and $\Psi = 0.01$.

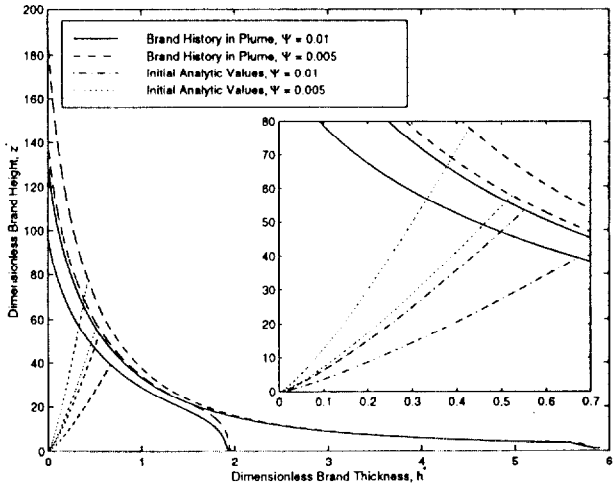

Figure 4 Plot of dimensionless brand thickness history as a function of lofting height for $\Psi = 0.01$ and 0.005 and $h_o^* = 2$ and 6. Also shown are the curves for the dimensionless initial propagation height as a function of dimensionless initial propagation thickness for $\alpha = 35°$ and $U_w^* = 4$. The maximum propagation will occur for those values where the curves intersect.

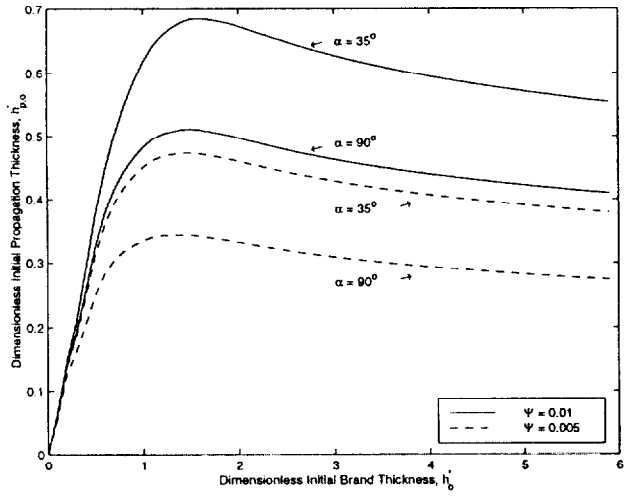

Figure 5 Dimensionless initial propagation thickness as a function of dimensionless initial brand thickness for $\Psi = 0.01$ and 0.005 and $\alpha = 90°$ and 35°, as calculated by the analytic equations. Note that the abscissa gives the thickness prior to lofting, while the ordinate gives that prior to propagation. The initial propagation thickness is independent of U_w^*.

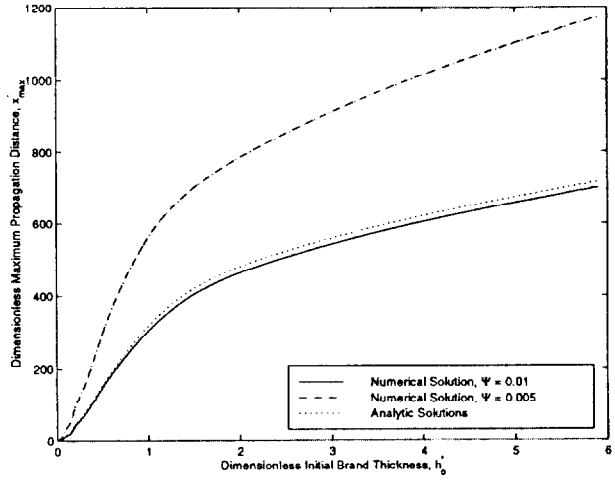

Figure 6 Comparison of the dimensionless maximum propagation distances calculated numerically and analytically as functions of dimensionless initial brand thickness, for $\Psi = 0.01$ and 0.005, $U_w^* = 4$, and $\alpha = 35°$. The analytic and numeric solutions for $\Psi = 0.005$ are indistinguishable.

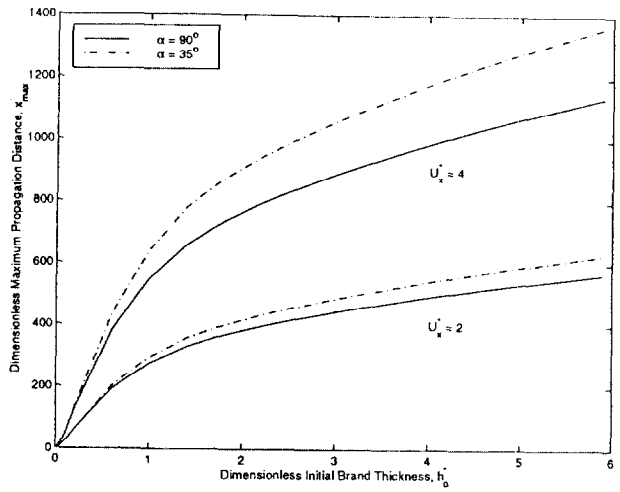

Figure 7 Three-dimensional plot of the dimensionless maximum propagation distance as a function of angle of attack and dimensionless initial brand thickness, with $U_w^* = 4$ and $\Psi = 0.01$. Maximum propagation for a given h_o^* occurs when $\alpha = 35°$.

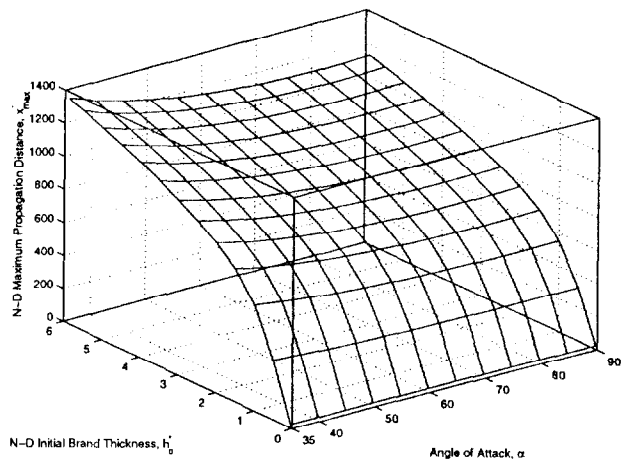

Figure 8 Three-dimensional plot of dimensionless maximum propagation distance as a function of burning parameter and dimensionless initial brand thickness, with $U_w^* = 4$ and $\alpha = 35°$.

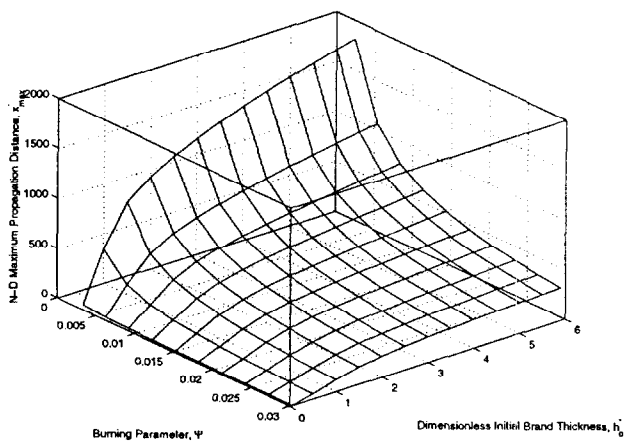

Figure 9 Three-dimensional plot of dimensionless maximum propagation distance as a function of burning parameter and dimensionless initial brand thickness, with $U_w^* = 2$ and $\alpha = 35°$.

NOTATION

A_c	Cross-sectional area of brand
B_o	Brand volume-to-surface-area ratio
B	Mass transfer number, $\left(QY_{o\infty}/\nu_o M_o - h_w\right)/L$
C	Coefficient for force equations, Eqs. (4, 6, and 7)
c_p	Specific heat of air
d, D	Brand diameter
F	Force
h	Brand thickness
$\bar{h}$	Average brand thickness
h_o	Total heat transfer coefficient
h_w	Specific enthalpy
$\hat{i}$, $\hat{k}$	Unit vectors in x- and z-directions
k_o	Brand thermal conductivity
m	Brand mass
M_o, M_f	Molecular weights of oxidizer and fuel
L	Effective latent heat of pyrolysis
W	Velocity of brand relative to its surroundings
U	Velocity of surroundings
f(0)	Initial value of dimensionless stream function, $f(0) = -0.353r^{-0.02}B^{0.611-0.0651\ln(B)}$
x	Propagation distance of particle from center of fire
Q	Energy released by combustion of vf moles of gas phase fuel
$\dot{Q}_O$	Rate of heat release for the fire
r	Mass consumption number, $Y_{o\infty}s/Y_{fw}$
R	Disk radius
s	Stoichiometric ratio, $\nu_f M_f/\nu_o M_o$
t	Time
T_∞	Ambient temperature
w_f	Brand terminal velocity
V	Particle velocity relative to ground
Y	Mass fraction
z	Vertical height of particle

GREEK

α_o	Brand thermal diffusivity
α	Angle of attack between disk and relative velocity vector
Γ	Angle between x-axis and relative velocity vector
ε	Length-to-diameter ratio
ν	Kinematic viscosity of air
ν_o, ν_f	Stoichiometric coefficients of oxidizer and fuel
ρ	Density
σ	Radial coordinate on disk surface

SUBSCRIPTS AND SUPERSCRIPTS

a	Air
bm	Baum & McCaffrey
c	Characteristic
d	Drag
fw	Disk surface
g	Gravity
ign	Time of ignition
l	Lift
max	Maximum
n	Normal
o	Initial
o∞	Ambient, oxidizer
p	Propagation
s	Solid
w	Wind
x, z	Component in x- or z-direction
*	Dimensionless

DIMENSIONLESS GROUPS

Fo	Fourier number, $\alpha_o t/B_o^2$
Bi	Biot number, $h_o B_o/k_o$